

# Absence of weak antilocalization in ferromagnetic films

N. Kurzweil, E. Kogan, and A. Frydman

*The Department of Physics, Bar Ilan University, Ramat Gan 52900, Israel*

(Dated: November 5, 2018)

We present magnetoresistance measurements performed on ultrathin films of amorphous Ni and Fe. In these films the Curie temperature drops to zero at small thickness, making it possible to study the effect of ferromagnetism on localization. We find that non-ferromagnetic films are characterized by positive magnetoresistance. This is interpreted as resulting from weak antilocalization due to strong Bychkov-Rashba spin orbit scattering. As the films become ferromagnetic the magnetoresistance changes sign and becomes negative. We analyze our data to identify the individual contributions of weak localization, weak antilocalization and anisotropic magnetoresistance and conclude that the magnetic order suppresses the influence of spin-orbit effects on localization phenomena in agreement with theoretical predictions.

PACS numbers: 72.15.Rn, 73.61.At, 75.70.Ak

## I. INTRODUCTION

Ferromagnetic thin films are of great interest because of their application in various areas of magnetoelectronics, magnetic read-heads, field sensors, random access memory elements and others. Most of the research effort is concentrated on ultraclean films which are advantageous for devices. However, disordered films are interesting from the scientific point of view since they allow to study the interplay between magnetization and localization. Like in normal metals, the semi-classical Drude conductivity at low temperatures is expected to be strongly influenced by quantum corrections.

Quantum corrections to electrical conductivity of normal metals were extensively studied in the past three decades. These corrections, derived from quantum interference between self-intersecting paths [1], are always negative in the case of purely potential scattering. When in addition to the potential scattering there exists spin-orbit (SO) scattering or magnetic-impurity scattering (scattering due to magnetic impurities in a paramagnetic metal) the situation becomes less definite. The interference may be constructive or destructive depending on the strength of the SO interaction [2–4]. In the general case the conductivity correction  $\delta\sigma$  can be presented as [5]

$$\delta\sigma = -\frac{2e^2 D_0}{\pi\hbar L^d} \sum_Q \left( \frac{\frac{3}{2}}{D_0 Q^2 + \frac{4}{3\tau_{SO}} + \frac{1}{\tau_\varphi}} - \frac{\frac{1}{2}}{D_0 Q^2 + \frac{1}{\tau_\varphi}} \right), \quad (1)$$

where  $D_0$  is the diffusion constant in  $d$  dimensions,  $L$  is the size of the sample,  $\tau_{SO}$  is the spin-orbit relaxation time, the inverse of which measures the strength of the SO interaction, and  $\tau_\varphi$  is the dephasing time. The first term in Eq. (1) is the contribution from the triplet channel, describing the constructive interference and leading to weak localization (WL). The second term is the contribution from the singlet channel, describing

the destructive interference and leading to weak antilocalization (WAL). This becomes even more obvious when one calculates the  $\mathbf{Q}$  sum and obtains [8]

$$\frac{\delta\sigma_d}{\sigma_d} \sim - \int_\tau^{\tau_\varphi} \frac{\lambda^2 v dt}{a^{3-d} (D_0 t)^{d/2}} \left( \frac{3}{2} e^{-t/\tau_{SO}} - \frac{1}{2} \right) \quad (2)$$

where  $\lambda$  and  $v$  are the (Fermi-surface) electron wave length and velocity respectively, and  $a$  is the film thickness or the wire radius. For  $d = 2$  one obtains

$$\begin{aligned} \delta\sigma_2 &\sim \frac{e^2}{\hbar} \left( -\ln \frac{\tau_\varphi}{\tau} \right), & \tau_{SO} \gg \tau_\varphi \\ &\sim \frac{e^2}{\hbar} \left( -\frac{3}{2} \ln \frac{\tau_{SO}}{\tau} + \frac{1}{2} \ln \frac{\tau_\varphi}{\tau} \right), & \tau_{SO} \ll \tau_\varphi, \end{aligned} \quad (3)$$

where  $\tau$  is the momentum relaxation time. As seen from Eq. (3), the spin-orbit scattering reverses the sign of the quantum correction to conductivity.

Both WL and WAL are suppressed by an applied magnetic field. An asymptotic estimate for magnetoconductance can be found from Eq. (2) taking into account that the upper limit of integration should now be  $t_H$  instead of  $\tau_\varphi$  if  $t_H \ll \tau_\varphi$ , where  $t_H \sim l_H^2/D_0$ , and  $l_H = (\hbar c/2eH)^{1/2}$  is the magnetic length. It is easy to see that in the absence of spin-orbit scattering the magnetoresistance (MR - the inverse of the magnetoconductance) is always negative. Substituting  $D_0 = \frac{1}{3} \frac{l^2}{\tau}$  yields the following expression for the magnetoconductance due to WL [5]:

$$\frac{\Delta\sigma_{WL}}{\sigma(0)} = -\frac{3}{2k_F^2 a l} \left\{ \psi \left( \frac{1}{2} + \frac{3}{4} \frac{l_H^2}{l^2} \right) - \psi \left( \frac{1}{2} + \frac{3}{4} \frac{l_H^2}{l_\varphi^2} \right) \right\} \quad (4)$$

where  $k_F$  is the Fermi wave length,  $l$  is the mean free path and  $l_\varphi$  is the dephasing length.

The situation is more complicated for WAL when spin-orbit scattering is important. In weak magnetic fields and under strong spin-orbit scattering the magnetoconductance reverses its sign and is given by

$$\frac{\Delta\sigma_{WAL}}{\sigma(0)} = -\frac{3}{4k_F^2 dl} \left\{ 2\psi \left( \frac{1}{2} + \frac{3l_H^2}{4l^2} \left[ 1 + \frac{l^2}{l_{SO}^2} \right] \right) - 3\psi \left( \frac{1}{2} + \frac{3l_H^2}{4l^2} \left[ \frac{l^2}{l_\varphi^2} + \frac{4}{3} \frac{l^2}{l_{SO}^2} \right] \right) + \psi \left( \frac{1}{2} + \frac{3l_H^2}{4l_\varphi^2} \right) \right\}. \quad (5)$$

where  $l_{SO}$  is the spin-orbit interaction length. As the magnetic field increases and becomes larger than

$$H_{SO} \simeq \frac{c\hbar}{e} \frac{1}{D_0\tau_{SO}} \quad (6)$$

the magnetoresistance becomes negative even in the presence of SO [8]. Similar to paramagnetic impurity scattering, SO interaction may result from lack of inversion symmetry which is described by the Dresselhaus term [9] or reduced dimensionality of the system related to the Bychkov-Rashba Hamiltonian [10].

From Eq. (1) it is clear that a quantity of crucial importance for the calculation of the quantum correction to the conductivity is the dephasing time  $\tau_\varphi$ . As well known, in low dimensionality conductors ( $d \leq 2$ ) for low enough temperatures  $\tau_\varphi$  is determined by electron-electron interaction involving small energy transfer,  $\omega \sim \tau_\varphi$ , and has the form [7, 8]

$$\frac{1}{\tau_\varphi} \sim \left( \frac{T}{D_0^{d/2} \nu_d \hbar^2} \right)^{2/(4-d)} \begin{cases} \ln \frac{p_F^2 l a}{\hbar^2}, & d = 2 \\ 1, & d = 1 \end{cases}, \quad (7)$$

where  $\nu_d$  is the density of states,  $p_F$  is the Fermi momentum.

One may ask, how do the above quantum corrections manifest themselves in the case where the metal is a ferromagnet. Dugaev et al. [11] theoretically studied the influence of ferromagnetism on WL and WAL phenomena. Qualitatively, the main idea in this work is that strong magnetic polarization in ferromagnetic materials excludes processes with the singlet Cooperon, which are responsible for the antilocalization in nonmagnetic materials with SO scattering. As a result, the quantum correction to conductivity is always negative in ferromagnetic samples and leads to negative magnetoresistance. This is due to the fact that in ferromagnetic materials ferromagnetic  $s-d$  exchange yields spin splitting which is comparable or larger than the thermal energy or the Landau level splitting due to magnetic field [6]. The resulting spin polarization of the conduction electrons influences the spin-flip scattering.

For the case of a 2D ferromagnetic film, which is relevant for our experiment, the results depend upon the orientation of the magnetization relative to the plane of the film. The easier is the case of the magnetization perpendicular to the plane. In this case the spin-flip scattering, which leads to weak antilocalization is totally suppressed. Thus, even in the presence of strong SO interaction the correction to conductivity and the magnetoresistance are

negative, hence there is only weak localization correction [6, 11]. When the magnetization is in plane, spin-flip scattering is present in the system, and one has to include the spin-flip processes in the Cooperon ladder. However, the overall quantum correction to the conductivity turns out to be of WL type, though smaller than in the case of magnetization perpendicular to the plane.

In this paper we describe a systematic experimental work designed to study the effect of ferromagnetism on localization phenomena. For this we use disordered amorphous films of ferromagnetic Ni and Fe in which we vary continuously the thickness and disorder of each sample. These films show a drop of the Curie temperature to zero at low film thickness [12]. This allows us to study the conductivity of a *single* sample - with and without ferromagnetism - in the temperature regime in which localization is important. We find that in the paramagnetic phase of our ultrathin film, the conductivity is governed by WAL as a result of strong Bychkov-Rashba SO scattering leading to positive MR. When the samples become ferromagnetic the magnetoresistance curves change sign and become negative, indicating that WAL is masked by magnetic effects in agreement with Dugaev et al.

## II. EXPERIMENTAL

In order to achieve substantial localization effects one would like to employ disordered metallic thin layers. For this reason we used ultrathin amorphous films in which the low thickness enhances the role of disorder and thus increases the affect of localization. The samples studied in this research were films of Ag, Ni and Fe with thickness varying between 0.05 and 12 nm and resistances between 1 M $\Omega$  and 100  $\Omega$ . The samples were fabricated using the technique of "quench condensation", i.e. thermal evaporation on a cryocooled substrate. This technique allows to deposit sequential layers of ultrathin films and measure transport without thermally cycling the sample or exposing it to atmosphere. This is particular advantageous for the study of thin ferromagnetic films such as Ni or Fe in which one would like to prevent rapid oxidation characteristic of these materials [13, 14]. Prior to the cooldown, six gold leads were evaporated on an insulating Si/SiO substrate. A mechanical mask was used to obtain a desired hall bar geometry enabling hall effect and 4 probe conductivity measurements on a 2 by 2 mm sample. The substrate was then connected to the He3 pot of a He3 fridge which was pumped to high vacuum to allow film evaporation. An insulating underlayer of Ge or Sb was predeposited prior to the metal evaporation while the substrate was held at T=4 K. This insulating layer wets the substrate enabling to achieve ultrathin continuous amorphous films even at monolayer thickness [15, 16]. An ultrathin metal film was then evaporated on the cold substrate. Deposition rate and film thickness were non-

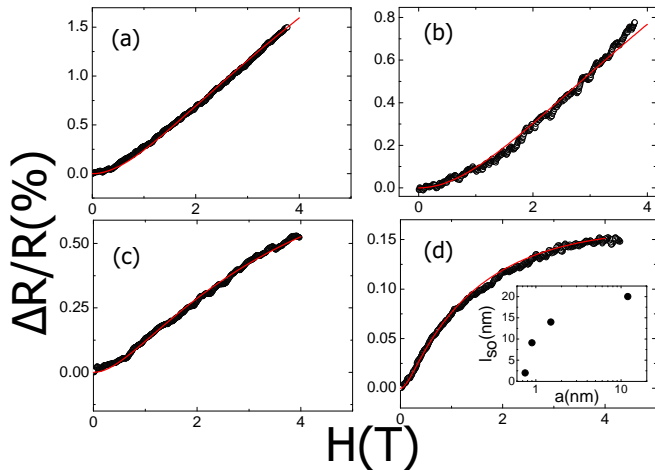


FIG. 1: MR curves of an Ag sample having various thickness, a. T=4.2 K. Solid lines are fits to WAL (Eq. 5) with mean free path of 0.2 nm. (a)  $a = 0.75$  nm. (b)  $a = 0.9$  nm. (c)  $a = 1.5$  nm. (d)  $a = 12$  nm. The inset shows the extracted  $l_{SO}$  as a function of thickness.

itored, in situ, by a quartz-crystal and sample resistance was measured during the growth. The evaporation was terminated at a desired thickness and resistance allowing transport measurements at different disorder states of the sample. The magnetotransport measurements presented in this paper were performed in the 25 K - 300 mK temperature range. A magnetic field up to 6 T was applied perpendicular to the substrate plain.

Previously [12] we studied the conductivity versus thickness of similar ultrathin films while driving them from strong to weak localization. Our analysis indicated that as the film is thickened, the microscopic properties such as mean free path,  $l$ , diffusion constant,  $D_0$ , or dephasing length,  $l_\varphi$  do not change. The parameter that is mainly affected by the thickness is the localization length  $\xi$  which is reduced due to the low dimensionality of the layer. Changing the thickness causes a crossover from strong to weak localization via the crossover from  $\xi < l_\varphi$  to  $\xi > l_\varphi$ .

### III. RESULTS AND DISCUSSION

As noted above, this research concentrates on the transport properties of ultrathin films of Ni and Fe for the purpose of investigating the influence of ferromagnetism on localization effects. For reference we studied the properties of non-ferromagnetic systems i.e. ultrathin layers of Ag. MR curves of a single Ag sample for several thicknesses are shown in fig. 1. It is seen that Ag layers exhibit a positive MR for all the studied thickness range. This result is indicative of films characterized by strong spin orbit interaction and thus exhibiting WAL. We attribute these results to the presence of a strong

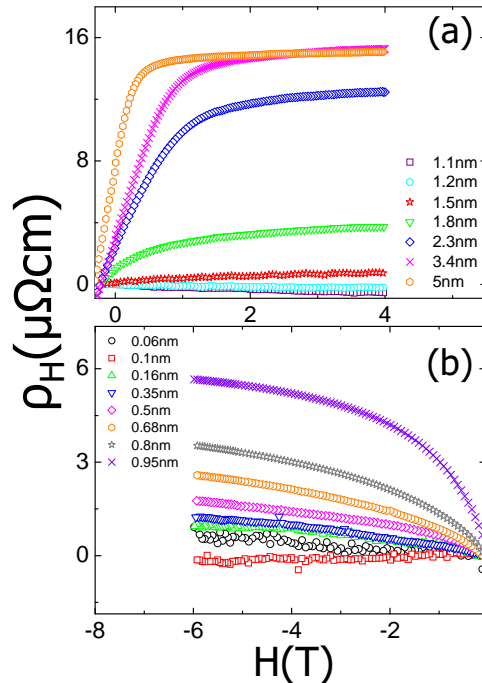


FIG. 2: Hall Effect measurements of sequential quench condensed Ni (a) and Fe (b) films. T=4.2 K.

Bychkov-Rashba term in which SO interaction is due to scattering on the surface caused by reduced dimensionality in the ultrathin film. The solid lines in fig. 1 are fits to WAL (Eq. 5). The extracted spin-orbit length,  $l_{SO}$ , grows with the layer thickness (see inset) demonstrating that the SO interaction becomes weaker as the films become thicker, in consistency with the assumption that Bychkov-Rashba scattering is the main contribution to the SO effects.

The situation is different for ferromagnetic layers. As described in Ref. [12], thin amorphous layers of Ni or Fe show no signs of ferromagnetism below a critical thickness,  $a_C$ , which is material dependent. As the thickness is increased the Curie temperature increases rapidly from zero to the bulk value. This means that for a given temperature one can observe a transition from paramagnetism to ferromagnetism as a function of thickness.

The measurement of magnetization in quench condensed films is somewhat problematic since the samples can not be heated to room temperature without affecting their geometry, hence conventional methods such as SQUID measurements are not relevant. For this reason we use the hall effect (HE) for which ferromagnetic films are characterized by a large contribution from the extraordinary hall effect (EHE) proportional to the magnetization. Fig. 2 shows Hall effect measurements at T=4.2 K for sequential layers of Ni and Fe films. These show that a measurable extraordinary Hall effect (EHE) con-

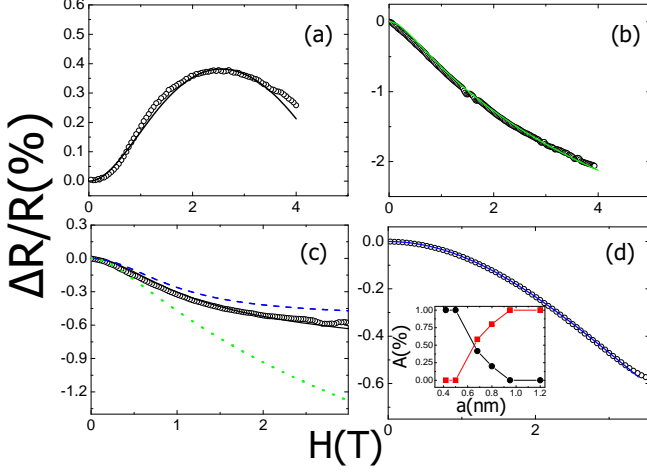


FIG. 3: MR curves of a Fe sample having various thickness  $a$ .  $T=4.2$  K. (a)  $a = 0.16$  nm. The solid line is a fit to WAL (Eq. 5). (b)  $a = 0.5$  nm. The solid line is a fit to WL (Eq. 4). (c)  $a = 0.8$  nm. The solid line is a fit to combination between WL (the dotted line) and AMR (the dashed line) of Eq. 9. (d)  $a = 7$  nm. The solid line is a fit to AMR (Eq. 8). The inset show the amplitudes of WL (circles) and AMR (squares) ( $A_{WL}$  and  $A_{AMR}$  of Eq. 9) as a function of the thickness.

tribution, which characterizes ferromagnetism, is absent for  $a < a_C$ , where  $a_C$  is 1.8 nm for Ni and 0.45 nm for Fe. Thus we can identify two regimes: For  $a > a_C(T)$  the films are ferromagnetic while for  $a < a_C(T)$  they show no spontaneous magnetization.

It turns out that this crossover from ferromagnetic to non ferromagnetic behavior has a striking effect on the magnetoresistance. At  $a = a_C$  the MR changes sign from positive to negative. Fig. 3 depicts MR curves for a number of growth stages of a Fe film, one for  $a < a_C$  and the rest for  $a > a_C$ . In the first stage the MR is positive and is very similar to the results obtained for Ag films having the same thickness. Here we obtain good fits to WAL (solid line). As  $a$  becomes larger than  $a_C$  and the films are characterized by spontaneous magnetization, the MR changes sign to negative, unlike the situation in Ag. For the first few monolayers of thickness above  $a_C$  the MR can be well fitted to WL without the influence of SO in accordance with Eq. 4 (fig 3b).

As the film is thickened the curves can not be fitted by assuming WL contribution alone any more. For thick enough ferromagnetic films we found [12] that the MR curves are best described by anisotropic magnetoresistance (AMR) characteristic of ferromagnetic films. The AMR effect relates the resistance value to the angle,  $\theta$ , between the the current and the magnetization [17]. The dependance of the resistance on  $\theta$  is known to be:  $\rho \propto \cos^2 \theta$ , where the resistance is maximum when the magnetization is parallel to the current. In our system

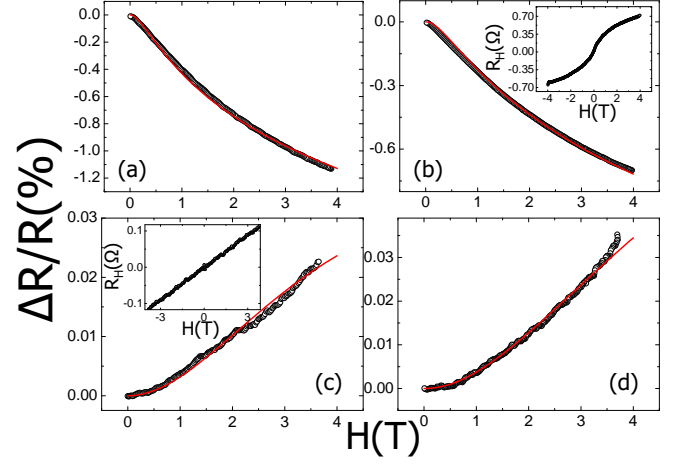


FIG. 4: MR curves of a 1.8 nm Ni film measured at the following temperatures: (a) 0.5 K (b) 1.7 K (c) 14 K, (d) 18 K. Solid lines in (a) and (b) are fits to Eq. 9. Solid lines in (c) and (d) are fits to WAL (Eq. 5).  $l_\varphi$  extracted from the fits are: 61.9, 48.9, 17.8 and 17.4 nm respectively. The insets in (b) and (c) are HE measurements.

the applied magnetic field is always directed perpendicular to the current. At zero field, both the magnetization and the current are in the sample plane. As the applied field is increased, the magnetization is rotated out of the plane thus increasing  $\theta$ . At the saturation field,  $H_S$ , the magnetization is parallel to the applied field and perpendicular to the current causing the resistivity to be minimal. In order to analyze our data we assume quadratic dependance of  $\Delta R$  on  $H$  at fields lower than  $H_S$  and saturation value at high fields, and use the following phenomenological expression:

$$\Delta R_{AMR} = \Delta R(\infty) \frac{H^2}{H^2 + H_S^2} \quad (8)$$

The solid line in fig 3d is a fit to this expression where  $H_s$  is taken from the Hall effect measurements such as those of figure 2. Hence, it appears that for thick enough ferromagnetic films the large contribution of AMR overshadows all of other MR effects such as that of weak localization.

In the intermediate regime (fig 3c), we fit the data to the combination between the two effects:

$$\Delta R_{com} = A_{AMR} \Delta R_{AMR} + A_{WL} \Delta R_{WL} \quad (9)$$

Where  $A_{AMR}$  and  $A_{WL}$  are coefficients determining the relative weight of the two effects and  $R_{WL} = 1/\sigma_{WL}$ . The inset in fig. 3 which depicts the dependence of  $A_{AMR}$  and  $A_{WL}$  on the thickness demonstrates that, for low thickness, the negative MR observed in the ferromagnetic state is mainly due to WL effects. As the film is thickened

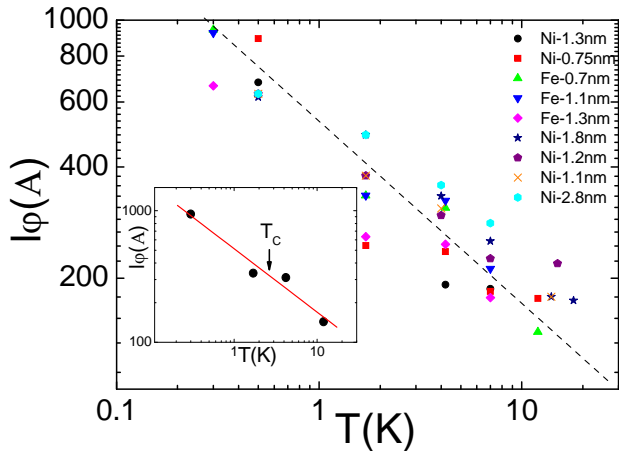


FIG. 5: Dephasing length,  $l_\phi$  as a function of  $T$  for a number of Ni and Fe samples having different thicknesses. The dashed line has a slope of  $-0.5$  and is a guide to the eye. The inset is an example of one Ni sample of  $0.7$  nm thick exhibits  $l_\phi \sim T^{-0.5}$ .

the relative AMR contribution grows and becomes the dominant factor for large thickness.

The above experimental results are consistent with the theoretical prediction of Dugaev et al [11]. For non-magnetic films, the MR curves are always positive, presumably as a result of the corrections of SO interactions on WL. For ferromagnetic films the MR is always negative. The analysis of the data show that the appearance of ferromagnetism in the film suppresses the effect of SO such that only the usual negative MR typical to WL is present.

Fig 3 demonstrated a transition from paramagnetic to ferromagnetic behavior as a function of thickness at constant temperature. A similar effect can be observed at constant thickness as a function of temperature. This is shown in fig. 4 which depicts MR and HE measurements of a  $1.8$  nm thick Ni film at different temperatures. For  $T < 4$  K (4a and 4b) the samples are ferromagnetic, as demonstrated from the observed EHE, and the MR is negative. In this regime the data fit a combination of WL and AMR of Eq. 9. For  $T > 4$  K (4c and 4d) only the ordinary HE can be observed, indicating that the film has lost its ferromagnetism. Indeed, in this regime the MR is positive and fits WAL behavior dominated by SO.

Fits to WAL and WL similar to those of fig. 4 enable to extract the values for the dephasing length,  $l_\phi$ , at different temperatures. It turns out that these values are very similar for Ni and Fe. Fig. 5 shows  $l_\phi$  versus  $T$  for 9 samples of Ni and Fe having different thicknesses. All films exhibit  $l_\phi \sim T^{-\alpha}$ , with  $\alpha$  ranging between  $0.3$ - $0.5$ . This power law is maintained even when the sample crosses over from ferromagnetism to paramagnetism and the MR changes sign. This is demonstrated in the inset which presents a  $0.7$  nm Ni film in which  $\alpha \sim 0.5$ .

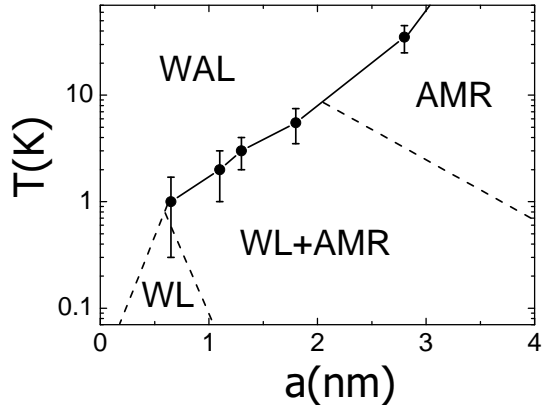


FIG. 6: A schematic illustration of the different MR regimes. The circles are the measured Curie temperatures,  $T_C$  as a function of thickness for a typical Ni film. The solid line connecting them separates between positive MR and negative MR. The dashed lines represent the estimated qualitative separation between regimes of different contribution to the negative MR

The crossover from WL to WAL, noted by the arrow in the figure, is not sensed by  $l_\phi$  which shows a smooth dependence on temperature. This behavior reinforces our confidence in the fitting procedure.

#### IV. CONCLUSIONS

In summary, we studied experimentally the magnetoresistance of ultrathin films of amorphous Ni and Fe. The Curie temperature for the ultrathin films of ferromagnetic metals decreases with the decrease of the film thickness, and can be arbitrary low or even zero making it possible to study both the paramagnetic state and the ferromagnetic state in the same sample, at low enough temperatures so that localization effects are prominent. The main results of this paper are illustrated in fig. 6 in which a schematic "phase diagram" is plotted. These can be summarized by the following findings: At temperatures larger than the curie temperature, in which the system shows no spontaneous magnetization, the MR is positive and is attributed to weak antilocalization. This is interpreted as signs for the fact that in the paramagnetic phase the magnetoresistance is determined by the magnetic field dependence of the quantum corrections to the conductivity in the presence of strong Bychkov-Rashba SO scattering. This corresponds to the WAL region on the "phase diagram". At temperatures smaller than  $T_C$ , the film becomes ferromagnetic and, at the same time, the MR curves change sign and becomes negative. For low enough temperature or thickness the MR curves follow the simple weak localization behavior without SO scattering (corresponding to the WL regime of

fig. 6). This indicates that scattering in the triplet channel, leading to WAL in the presence of SO scattering, is suppressed, and only scattering in the singlet channel is effective. As the film is thickened or temperature raised the magnetoresistance due to quantum correction to the conductivity is masked partially or completely by the anisotropic magnetoresistance effects. This corresponds to WL+AMR and AMR regions on the “phase diagram” respectively.

Thus we have found that ultrathin films of amorphous Ni and Fe, interesting by itself due to possible applications, can serve as a testing ground for the theory of quantum corrections to the conductivity. The experimental results agree qualitatively with the theoretical prediction [11] that ferromagnetism in a film totally suppresses the influence of spin orbit scattering on the perpendicular magnetoresistance. Though there is no theory discussing the interplay between the different contributions of WL and AMR to the magnetoresistance curve in such films, the analysis of the experimental results provides information about the smooth transition from the WL dominated regime to the region in which AMR governs the behavior.

We are grateful for useful discussions with L. Klein. This research was supported by the Israeli academy of science (grant number 399/09)



[1] For reviews see, e.g., G. Bergmann, Phys. Rep. **107**, 1 (1984); P. A. Lee and T. V. Ramakrishnan, Rev. Mod.

- Phys. **57**, 285 (1985).  
 [2] P. W. Anderson, E. Abrahams and T. V. Ramakrishnan, Phys. Rev. Lett. **43**, 718 (1979).  
 [3] S. Hikami, A. I. Larkin and Y. Nagaoka, Prog. Theor. Phys, **63**, 707 (1980).  
 [4] S. Maekawa and H. Fukayama, J. Phys. Soc. Jpn. **50**, 2516 (1981).  
 [5] J. Rammer, *Quantum Transport Theory*, Perseus Books, Reading, MA, 1998.  
 [6] S. Sil, P. Entel, G. Dumpich, and M. Brands, Phys. Rev. **72**, 174401 (2005).  
 [7] B. L. Altshuler, A. G. Aronov, and A. D. Khmel'nitskii, Solid State Comm. **39**, 619 (1981)  
 [8] B. L. Altshuler, A. G. Aronov, *Electron–Electron Interaction in Disordered Conductors*, Elsevier Science Publishers, 1985.  
 [9] G. Dresselhaus, Phys. Rev. **100**, 580 (1955).  
 [10] Yu.A. Bychkov and E. I. Rashba, Pis'ma Zh. Eksp. Teor. Fiz. **39**, 66 (1984).  
 [11] V. K. Dugaev, P. Bruno, and J. Barnaś, Phys. Rev. B **64**, 144423 (2001).  
 [12] N. Kurzweil, E. Kogan and A. Frydman, Phys. Rev. Lett. **102**, 096603 (2009).  
 [13] A. Frydman and R.C. Dynes, Sol. State Comm. **110**, 485 (1999).  
 [14] A. Frydman, T.L. Kirk and R.C. Dynes, Solid State Commun. **114**, 481 (2000).  
 [15] M. Strongin, R. Thompson, O. Kammerer and J. Crow, Phys. Rev. **B1**, 1078 (1970).  
 [16] D.B. Haviland, Y. Liu, and A.M. Goldman, Phys. Rev. Lett. **62**, 2180 (1989).  
 [17] T. R. McGuire and R. I. Potter, IEEE Trans. Magn. **11**, 1018 (1975).